ACS Sustainable Chemistry & Engineering

pubs.acs.org/journal/ascecg

Research Article

Accelerated Synthesis of a Ni_2Cl_2(BTDD) Metal–Organic Framework in a Continuous Flow Reactor for Atmospheric Water Capture

Sujay Bagi, Ashley M. Wright, Julius Oppenheim, Mircea Dincă, and Yuriy Román-Leshkov*

Cite This: https://dx.doi.org/10.1021/acssuschemeng.0c07055

Read Online

ACCESS | Metrics & More | Article Recommendations | Supporting Information

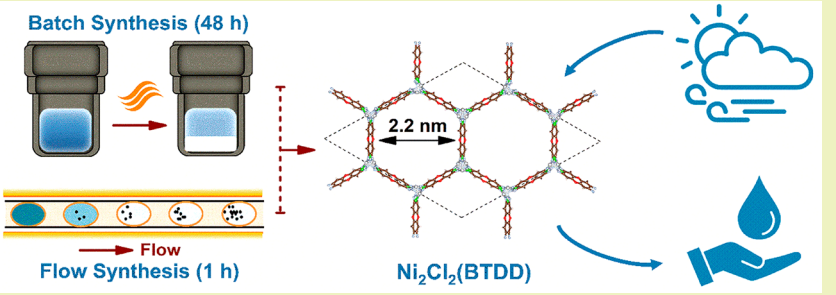

ABSTRACT: Atmospheric water capture (AWC) has tremendous potential to address the global shortage of clean drinking water. The Ni_2Cl_2(BTDD) metal–organic framework (MOF) has shown optimal water sorption performance under low relative humidity conditions, but its potentially high production costs, stemming in part from its lengthy multiday synthesis, has hindered widespread implementation. As with most traditional MOF syntheses, the original synthesis of Ni_2Cl_2(BTDD) involves batch reactors that have intrinsic inefficiencies impacting productivity during scale-up. We report a continuous manufacturing process for Ni_2Cl_2(BTDD) that can achieve higher yields, reduced solvent use, and drastically faster crystallization times in comparison to the batch process. Optimization of the synthesis space in the flow reactor as a function of residence time, temperature, and solvent volume yields 50% and 40% reductions in methanol and hydrochloric acid consumption by volume, respectively, with a simultaneous 3-fold increase in productivity (defined in units of kg_{MOF} $m^{-3}day^{-1}$). A computational fluid dynamics (CFD) model was developed to quantitate productivity enhancements in the flow reactor based on improved heat-transfer rates, larger surface-area to volume ratios, and effective residence times. This work adds critical facets to the growing body of research suggesting that the synthesis of MOFs in flow reactors offers unique opportunities to reduce production costs.

KEYWORDS: *Metal–organic frameworks, Continuous flow chemistry, Synthesis design, Atmospheric water capture, Scale-up*

INTRODUCTION

Most arid and semiarid regions in the world do not have access to potable water. This problem will worsen due to increasing global water demand for both personal and industrial use, a growing global population, and desertification of fertile areas through overfarming and climate change, eventually leading to a projected water deficit of almost 2000 billion m^3 by 2030.[1,2] In areas with relative humidity (RH) below ca. 30%, water harvesting relies on capital- and energy-intensive processes, such as dewing or seawater desalination supplemented with a complex distribution infrastructure of pipelines.[3,4] Atmospheric water capture (AWC) offers an alternative solution given that the atmosphere holds nearly 1.3×10^{16} L of water: a value representing ca. 0.3% of the global fresh water supply.[5,6] However, direct water capture from the atmosphere in areas with low RH (<30%) in an energy-efficient manner requires new sorbent materials. The ideal AWC sorbent material must have large gravimetric capacities, steep water uptake characteristics in a narrow RH range, and complete water release with minimal temperature swings over thousands of cycles.

Metal–organic frameworks (MOFs) fulfill many, if not all, of these requirements. MOFs are crystalline coordination lattices consisting of multitopic organic linkers and inorganic polynuclear clusters forming highly ordered 2D and 3D structures.[7] One class of MOFs that is attractive for AWC applications features coordinatively unsaturated open metal sites that serve as nucleation sites for water adsorption.[8] Recently, Dincă and co-workers[9−11] demonstrated that the M_2Cl_2(BTDD) (M = Co, Ni; H_2BTDD = bis(1H-1,2,3-triazolo[4,5-*b*],[4′,5′-i])dibenzo[1,4]dioxin) family of MOFs, which feature hexagonal pores decorated with open metal sites, are particularly well-suited for direct water capture from

Received: September 23, 2020
Revised: January 22, 2021

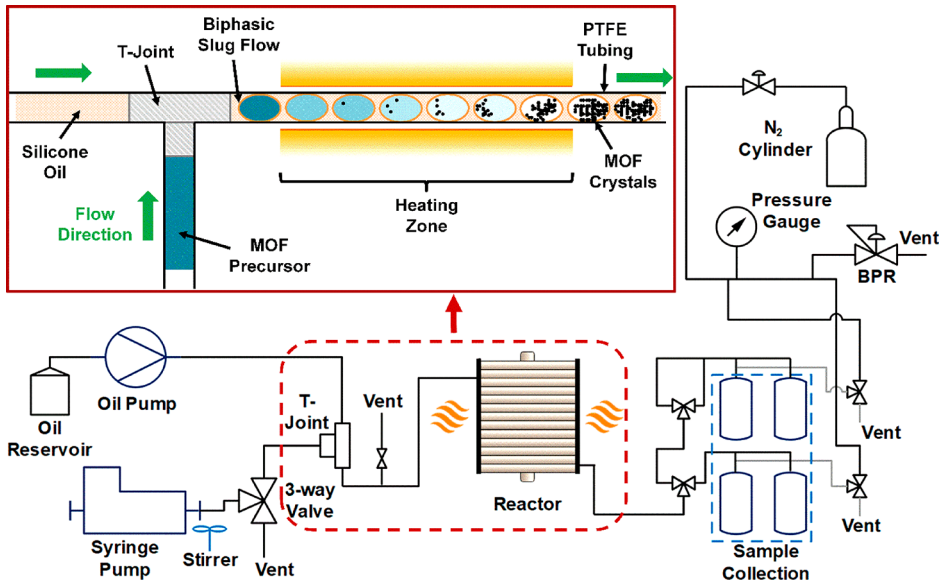

Figure 1. Schematic for the modular flow synthesis platform. Inset picture with red boundaries illustrates the phenomenological model of crystallization using a biphasic slug flow generated from two immiscible fluids in a T-junction.

simulated atmosphere. In particular, the Ni analog exhibits an exceptional gravimetric water uptake capacity of 1.07 $g.g^{-1}$ at a relative humidity (RH) of 35%.

The energy efficiency of water capture and release from Ni_2Cl_2(BTDD) was optimized by matching pore size to the critical diameter for water capillary condensation and minimizing adsorption/desorption hysteresis.[12,13] While being more expensive than other sorbents, such as silica gel and zeolites, MOFs are topologically diverse with tunable properties, making them ideally suited for water-capture applications.[14]

Despite its superior water uptake performance, scale-up of the manufacturing of Ni_2Cl_2(BTDD) remains prohibitively expensive due to long reaction times and large solvent volumes required for precursor dilution in the reaction mixture. For example, the synthesis of 1 g of Ni_2Cl_2(BTDD) requires the dissolution of 1.808 g of $NiCl_2{\cdot}6H_2O$ and 0.912 g of the organic ligand H_2BTDD in a solvent mixture comprising 800 mL of *N,N*-dimethylformamide (*N,N*-DMF), 800 mL of methanol (CH_3OH), and 512 mL of aqueous hydrochloric acid (HCl, 37 wt %), followed by heating at 100 °C for 48 h in a batch reactor to generate crystalline solids with ca. 75% yield. Slow crystallization times coupled with high solvent-to-solid ratios severely limit productivity, and this problem is exacerbated during scale-up due to inherent challenges associated with increasing the size of batch reactors.[15] These inefficiencies result in higher costs and considerable capital and operating expenditures to produce the quantities needed for industrial AWC applications.[16,17] It is therefore imperative to identify approaches that minimize synthesis costs through reduced use of solvents, increasing yields, and increasing process productivity for all MOFs, and for Ni_2Cl_2(BTDD) in particular.

The use of flow chemistry to achieve product intensification by improving heat and mass transfer, decreasing the use of solvents, and improving scalability through parallelization has transformed many disciplines, including polymer chemistry,[18] organic synthesis,[19−21] and photochemistry.[22] Numerous studies over the past decade have demonstrated the feasibility of synthesizing MOFs in flow;[23−31] however, the influence of synthetic parameters on product crystallinity and scale-up strategies for high-throughput manufacturing by considering transport processes have not been explored thoroughly. Here, we investigate the use of flow reactors for the accelerated synthesis of Ni_2Cl_2(BTDD) under mild solvothermal conditions. Specifically, we use a biphasic liquid−liquid slug flow pattern to perform continuous microbatch MOF crystallization that resulting in drastic increases in manufacturing productivity in comparison to batch processes. Computational fluid dynamics (CFD) calculations were used to quantitate productivity enhancements in the flow reactor based on improved heat-transfer rates, larger surface-area to volume ratios, and effective residence times. This information was used to model a scale-up scenario for producing 1 kg of Ni_2Cl_2(BTDD) per month, providing estimates for supply chain logistics and equipment sizing. This work demonstrates that synthesis in flow enables the manufacture of MOFs for AWC with significantly reduced materials costs and increased productivity compared to batch.

RESULTS AND DISCUSSION

Continuous MOF crystallization studies were performed in a flow reactor shown schematically in Figure 1. The injection module consists of a syringe pump and a positive displacement piston pump to introduce the precursor mixture and silicone oil, respectively. The reactor module is composed of PTFE tubing held together using an aluminum core and jacket, which is inserted into an electrically heated furnace allowing for nearly isothermal operation with fast heat transfer. A back-pressure regulator maintains the reactor operating pressure at a value higher than the bubble-point pressure of the reaction mixture. The MOF precursor mixture is injected into a continuous stream of silicone oil using a T-junction forming a segmented biphasic slug flow. Silicone oil was used because it preferentially wets the hydrophobic surface of the PTFE tubing, thereby producing a continuous phase for the MOF precursor mixture to travel as discrete, uniformly spaced droplets within the tube. In our flow reactor, the slug

https://dx.doi.org/10.1021/acssuschemeng.0c07055
ACS Sustainable Chem. Eng. XXXX, XXX, XXX−XXX

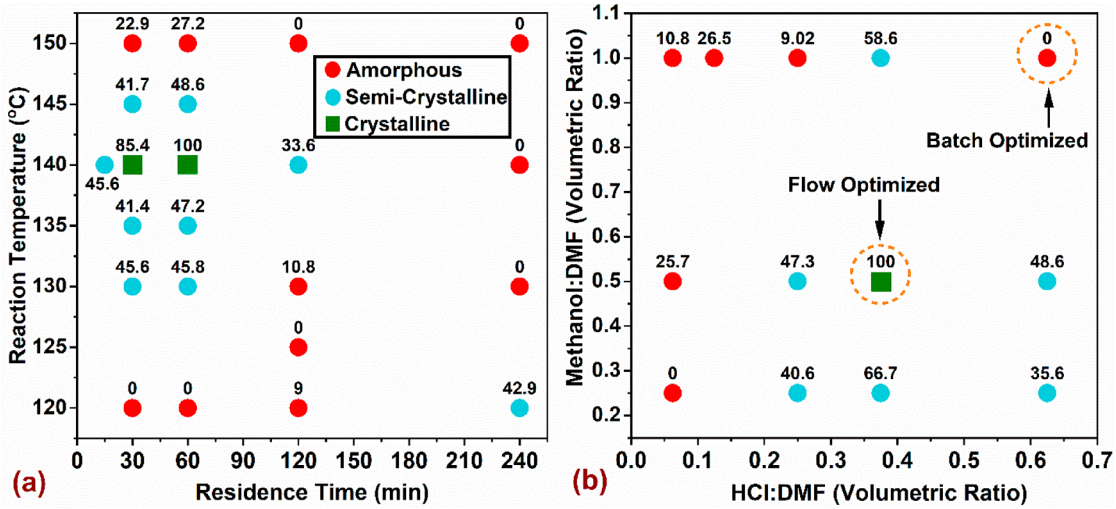

Figure 2. Map of synthesis space investigated for Ni_2Cl_2(BTDD) using flow synthesis varying (a) reaction temperature and residence time and (b) volumetric ratios of methanol/DMF and HCl/DMF solvents at a fixed temperature of 140 °C and 60 min residence time. Labels represent relative crystallinity in percentages (% RC), which were quantified by the intensity contribution in powder X-ray diffraction (PXRD) patterns originating from crystalline phase in the samples. The metal/ligand (M/L) molar ratio was maintained at 2.2 in all cases.

generation process is associated with the dynamic pressure profile existing at the T-junction when two immiscible fluids are simultaneously introduced in the stream. When the stream of the first phase is flowing through the junction, the flow of the second phase is obstructed due to immiscibility of the two phases, resulting in pressure build up. When the pressure reaches a critical point, the first phase is driven back from the T-junction shearing off the droplet into the stream, generating a slug. This alternated cyclic build-up and release of pressure is responsible for the segmentation of the liquids allowing reproducible slug lengths.[32,33]

Each slug is equivalent to a well-mixed microbatch reactor, where the interfacial properties between the two phases, such as surface tension and viscosity, control the shape and fluid dynamic properties of the droplet. Accordingly, in order to maintain a stable biphasic slug flow, the surface tension between the precursor and continuous phase should be lower than the surface tension between precursor and walls of reactor tubing.[34] Within each droplet, complete mixing of reagents is achieved through chaotic advection, where repeated folding and stretching of fluid layers accelerates diffusive mixing.[35,36] Importantly, compartmentalization of the MOF precursor in microliter volume droplets results in high surface area to volume (SA/V) ratios, which translates to shorter diffusion length scales for heat and mass transport processes. The slugs undergo a step-function change from room temperature to reaction set-point temperature upon entering the heated reaction zone. Precise temperature control is critical for manipulating the kinetics of nucleation, short-range crystalline ordering, and crystal growth.[37] Consequently, the flow system affords rapid mixing of reagents, near perfect step changes in temperature profiles, and precise control of residence times, all critical elements to accelerate nucleation and crystallization events.[34,38] Flow dynamics of precursor slugs with crystalline MOF solids at the outlet of the reactor operated at 140 °C and a residence time of 60 min are exemplified in Video S1. Importantly, this flow reactor setup supports a wide operational window to control the steady-state evolution of the product crystallinity by varying reaction conditions, including residence time (minutes to days) and temperature (up to 250 °C at a working pressure of 25 atm). Additional details pertaining to flow reactor components, operational windows, volumetric flow rates, and residence times are summarized in Figures S1, S2 as well as Tables S1, S2 of the Supporting Information.

Unlike batch reactors that intrinsically operate in a transient mode, flow reactors allow studies of the crystallization process at steady state with precise control over temperature and residence time.[16] These features enable time-resolved crystallization studies in a single experiment run. Figure 2 shows a map of the Ni_2Cl_2(BTDD) synthesis space where the effects of changing solvent ratio, residence time, and temperature on product crystallinity were investigated. The relative crystallinity (RC), determined from a ratio of intensity contributions originating from the crystalline phase that was calculated using an iterative background correction method to the total intensity from the PXRD patterns (Equation S1 and Figure S3 provide additional details), was used to define the amount of crystalline product per experiment.[39] Accordingly, a value of 100% RC corresponded to the highest yield of crystalline Ni_2Cl_2(BTDD), a value of >80% RC was classified as "crystalline", a value in the 30% ≤ RC ≤ 80% range was classified as "semi-crystalline", and RC values <30% were classified as "amorphous". Residence time and reaction temperature were varied in a range of 15−240 min and 120−150 °C, respectively, based on synthesis parameters previously reported in the literature.[23−26,31,40−42] Optimal Ni_2Cl_2(BTDD) crystallinity values were obtained for a reaction temperature of 140 °C and residence times between 30 and 60 min (Figure 2a). Temperatures above 150 °C resulted in linker degradation, while reactions below 120 °C failed to crystallize the MOF in the specified range of residence times. Note that residence times greater than 240 min were not investigated as they resulted in a lower process productivity (by a factor of 4 compared to flow conditions optimized at 60 min), making it unattractive in comparison to the batch process.

Flow reactors can usually operate at higher concentrations provided the reagents remain in solution: an advantage in the current scenario for using a concentrated precursor mixture to increase productivity while maintaining similar yields.[43,44]

https://dx.doi.org/10.1021/acssuschemeng.0c07055
ACS Sustainable Chem. Eng. XXXX, XXX, XXX−XXX

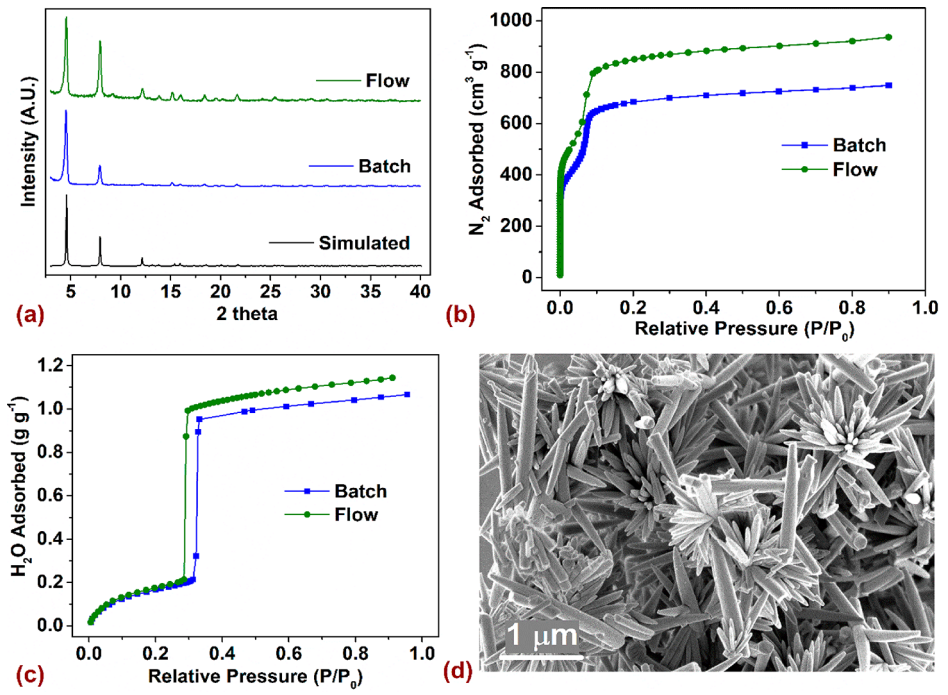

Figure 3. Characterization of $Ni_2Cl_2(BTDD)$ synthesized at optimal flow reaction conditions using (a) PXRD patterns, (b) N_2 adsorption isotherm at 77 K, (c) water vapor adsorption isotherm at 298 K, and (d) SEM image.

Figure 2b plots the results of varying the volumetric ratio of solvents (CH_3OH and HCl normalized to DMF) at 140 °C with a residence time of 60 min. Solvent composition was optimized starting from the recipe used in batch (1:1:0.64 volumetric ratio for DMF, CH_3OH, and HCl) and lowering HCl content by 10%, 40%, and 60% and CH_3OH by 25% and 50%. Interestingly, the solvent composition used in batch synthesis (labeled "Batch Optimized" in Figure 2b) resulted in amorphous residue in flow synthesis. The highest amount of crystalline solids in flow reactor was obtained with a volumetric ratio of DMF/CH_3OH/HCl = 1:0.5:0.38 (labeled "Flow Optimized" in Figure 2b). These values represent a decrease in CH_3OH and HCl volume by 50% and 40%, respectively, compared to the optimized batch composition. Additionally, we performed three batch syntheses at 100, 120, and 140 °C with a crystallization time of 48 h using the "flow optimized" starting composition. These results are compared to the samples synthesized in flow reactor under optimal conditions (140 °C, 1 h) using PXRD, N_2 adsorption, and water-uptake measurements (Figure S4 and Table S5). The BET surface area for batch samples steadily increased from 1795 to 1944 $m^2 \cdot g^{-1}$, as a function of reaction temperature (100 to 140 °C), while the gravimetric water uptake capacity steadily increased from 0.91 to 0.98 $g \cdot g^{-1}$ at 92% RH. The corresponding % RC values (Table S5) confirm an increase in crystallinity with higher temperature for batch samples, while flow synthesized samples exhibited the highest crystallinity of all synthetic conditions. Importantly, no solids are formed in batch syntheses after 1 h of crystallization. Taken together, these data demonstrate that the flow system can access unique synthetic conditions leading to $Ni_2Cl_2(BTDD)$ with a higher surface area and water-uptake, accompanied by a simultaneous reduction of solvents used and a lower residence time. We therefore conclude that the flow synthesis of $Ni_2Cl_2(BTDD)$ is advantageous in every aspect compared to batch synthesis.

In deprotonation modulation, the amount of modulator (HCl) has to be tuned in the reaction mixture based on the synthesis route and reaction conditions such as temperature and residence time. Under identical solvothermal conditions, reduction in the amount of modulator (HCl) accelerates the MOF formation process thus leading to a product with lower crystallinity, while an increase in modulator lowers crystallization rates of MOF thereby requiring longer residence times for crystal growth. Owing to small system dimensions and a large surface-area to volume ratio in the flow reactor that leads to fast heat transfer, the heating profiles achieved are different compared to those of the batch reactor which typically sees large gradients in heat and mass transfer. This is the primary reason for batch and flow syntheses exhibiting different optimal reaction conditions (temperature, time, and composition) to synthesize crystalline product. The amount of DMF could not be changed as it was maintained at the solubility limit of the H_2BTDD ligand in the precursor mixture. The metal salt and the ligand had a molar ratio of 2.2 (to keep a 10% stoichiometric metal excess) in all synthetic conditions explored in the design space. The yield obtained in batch and flow syntheses were ~75% and ~80%, respectively (Table S6), and are calculated based on the conversion of the limiting reagent (H_2BTDD ligand) into $Ni_2Cl_2(BTDD)$. The maximum productivity achieved in the batch synthesis was 0.245 kg_{MOF} $m^{-3}day^{-1}$ while flow synthesis resulted in 0.765 kg_{MOF} $m^{-3}day^{-1}$, representing a 3-fold productivity increase (Table S7). Flow synthesis productivity slightly decreases to 0.509 kg_{MOF} $m^{-3}day^{-1}$ if we take into account the silicone oil along with reaction mixture in our calculation. The standard engineering productivities based on reactor volume rather than volume of reaction mixture translates to 0.0643 kg_{MOF} $m^{-3}day^{-1}$ for batch and 12.24 kg_{MOF} $m^{-3}day^{-1}$ for flow, representing 2 orders of magnitude (~190 times) higher productivity achieved in flow (Table S7).

https://dx.doi.org/10.1021/acssuschemeng.0c07055
ACS Sustainable Chem. Eng. XXXX, XXX, XXX−XXX

Samples synthesized in flow at optimal reaction conditions were characterized using powder X-ray diffraction (PXRD), N_2 adsorption, scanning electron microscopy (SEM), transmission electron microscopy (TEM), and water uptake measurements and were compared with those of samples synthesized in batch. Figure 3a compares the reflections from PXRD patterns for Ni_2Cl_2(BTDD) synthesized in flow and batch along with a simulated pattern from the computational model, confirming the single-phase nature of the flow synthesized microcrystalline powder sample. The permanent porosity of activated samples synthesized using batch and flow method was studied using N_2 adsorption isotherms at 77 K (Figure 3b). The activated samples exhibit a Type IV isotherm, as is expected for mesoporous materials. To satisfy the first criteria of the BET equation,[45] isotherm data was fit to the 0.05−0.15 P/P_o range, yielding values of 1837 and 2157 $m^2.g^{-1}$ for batch and flow samples, respectively. Water vapor adsorption isotherms were measured at 298 K for the activated samples (Figure 3c). Both batch and flow samples exhibit Type IV isotherms with a steep uptake step at approximately 0.28 P/P_o, which is equivalent to 28% RH. At 92% RH, the total water uptake for batch and flow samples is 1.06 and 1.14 $g.g^{-1}$, respectively. Ni_2Cl_2(BTDD) crystallizes in the $R\bar{3}m$ space group (trigonal crystal system) with an olive green needle-shaped morphology of microcrystals confirmed by the SEM image in Figure 3d, identical to previously reported structure.[46,47] Samples synthesized in batch and flow are compared in Figure S5 using high-magnification SEM images, while Figures S6 and S7 provide high-resolution TEM images. Synthesis of Ni_2Cl_2(BTDD) in flow maintains similar crystallinity, pore size, and water-uptake characteristics compared to samples synthesized in batch, while reducing the volume of solvents used in the precursor mixture and an overall improvement in process productivity.

Although a large number of studies exist on novel MOF structures and their potential applications, there is a paucity of reports on the scale-up of MOF syntheses.[40,41,48,49] The key translation piece for the use of MOFs in revolutionary technology platforms is the ability to manufacture at desired scale and purity and satisfy market price requirements.[25] The design of scaled-up flow reactors as a manufacturing system involves the appropriate sizing of reactor equipment (such as pumps, reactor tubing configuration, heating furnace and sample collection strategy) and shorter crystallization times by optimization of synthetic conditions for higher throughput.[50] Although parallelization offers a simple method of linear productivity scale-up by increasing the number of reactors, it requires a complex network of fluid flow distribution and control devices.[51] Alternatively, throughput can be increased by enlarging the inner diameter (ID) of the reactor tubing, which results in quadratic dependence on volumetric flow rate ($Q \propto d^2$). An increase in tube ID by a factor of 4, from 1/16 in. (0.158 cm) to 1/4 in. (0.635 cm), increases the productivity by a factor of 16, assuming the yields are constant. However, the downside to this approach is the reduction in surface-area to volume ratio ($SA/V \propto d^{-1}$) of the tubing, which could decrease the efficiency of heat transfer processes.[33,40,41] From an operational standpoint, the propensity for hydrodynamic failure due to clogging of synthesized solids in the tube is indirectly proportional to the tube ID.[17] Accordingly, we modeled a scale-up scheme by enlarging the tube ID using the COMSOL Multiphysics platform to compute variation in heat transfer rates and growth of thermal boundary layers as a function of tube ID. The reactor is modeled as a 2D axisymmetric geometry and a coupled heat transfer and fluid flow problem is solved under a nonisothermal interface. Axial temperature profiles for different tube IDs as a function of the precursor position from reactor inlet as it traverses the heated reaction zone are shown in Figure 4a, while gradients in

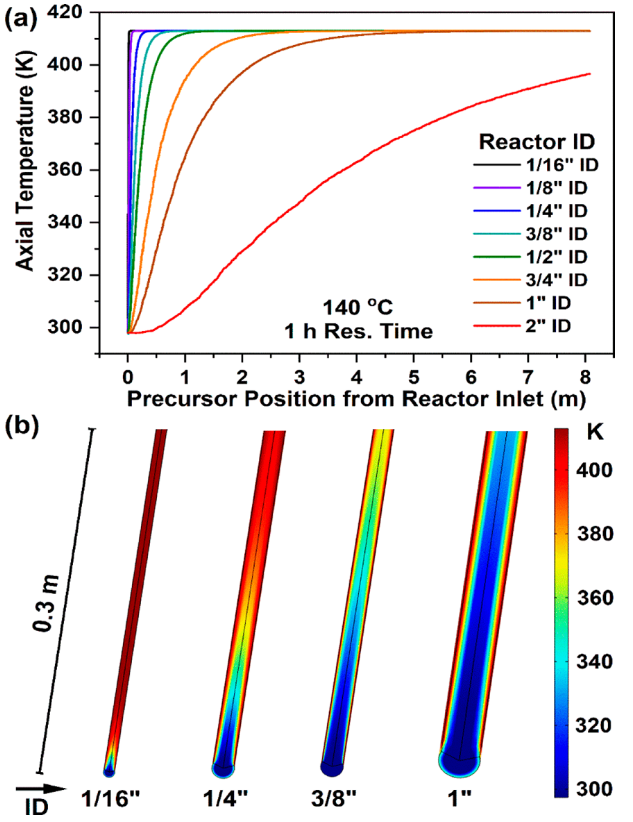

Figure 4. (a) Axial temperature profile along the length of reactor tube plotted against position of the precursor slug from reactor inlet. (b) Three dimensional (3D) slice plots at the entrance region of flow reactor showing both the temperature gradient and the growth of thermal boundary layers in the heated reaction zone as a function of tube ID. Outer diameter and tube wall is held at 140 °C, and fluid flow has linear velocity of 13.4 cm/min to achieve residence time of 60 min (8 m reactor tube length).

temperature near the entrance region of reaction zone and evolution of thermal boundary layers as a function of tube ID are illustrated in Figure 4b. The variation in heat transfer rates induces deviation in effective residence time (τ_{eff}), which is defined as the ratio of time spent by precursor at set point temperature in the reaction zone to the desired residence time. It was found that tube IDs below 3/8 in. have >90% τ_{eff}, while further increasing the tube ID results in poorer heat and mass transfer characteristics compared to those typically seen in batch reactor (Figure S10). Thus, owing to short diffusion length scales and high SA/V for tube IDs below 3/8 in. (0.952 cm), the fluid exhibits a near step-function change in the temperature from room temperature to the reaction temperature. The reactor tubing was modeled with uniform wall temperatures to characterize developing thermal boundary layers radially inward to the tube axis. The boundary layer thickness increases along the length of the tube and gradually fills the entire flow section. The distance from inlet to the region of boundary layer convergence is defined as thermal entrance length (L_T), beyond which there is no radial gradient

https://dx.doi.org/10.1021/acssuschemeng.0c07055
ACS Sustainable Chem. Eng. XXXX, XXX, XXX−XXX

in temperature.[52,53] The L_T for a 1/16 in. reactor is 2.1 cm, while a 1 in. reactor has an L_T of ∼5200 cm: an increase of 3 orders of magnitude when operated at the same reaction conditions (140 °C and 60 min res time). Owing to the small system dimensions in the case of 1/16 in. (radius of 0.079 cm), boundary layers quickly developed resulting in fast heat transfer characteristics and a high τ_{eff}. Details on meshing sequence and modeling parameters are summarized in Figures S8, S9 and Table S2.

Trade-offs associated with the enlargement of reactor tubes for higher production rate while losing the benefits of small system dimensions in the flow reactor must be judiciously considered before scale-up of the system. Computation of MOF production rates and the consumption of reagents with an increase in the tube ID are important from a standpoint of logistical planning while operating in a continuous manufacturing environment. A target scenario for synthesizing 1 kg of Ni_2Cl_2(BTDD) per month with continuous operation was evaluated and presented in Figure S11 and Table S3; additional assumptions are described in section 3 of the Supporting Information. On the basis of our heat transfer models, in order to maintain favorable heat and mass transfer characteristics, the reactor configuration must have a maximum ID of 3/8 in.. However, this configuration can only achieve ∼0.21 kg_{MOF} per month, while the reactor with 1/16 in. ID used in the current study synthesizes ∼0.00587 kg_{MOF} per month, 2 orders of magnitude lower. A resourceful strategy in this case would be a combinatorial approach of increasing tube ID to an extent, where heat transfer characteristics are retained, and parallelization of such reactor units, ensuring higher production rates. Estimates presented in Figure S11a require using 5 identical reactor units of 3/8 in. ID operated in parallel to achieve the target production scenario of 1 kg of Ni_2Cl_2(BTDD) per month. The traditional batch synthesis procedure employs a 1000 mL glass bottle, producing 260 mg of Ni_2Cl_2(BTDD) from 528 mL of reaction mixture heated at 100 °C for 48 h. A scale-up of the synthesis to manufacture 1 kg of Ni_2Cl_2(BTDD) would involve the usage of ca. 3847 bottles of 1000 mL capacity, each containing ca. 528 mL of reaction mixture. From an operational standpoint, replacing 3847 bottles of 1 L capacity with one large volume reactor vessel, for example, a 3500 L vessel with ∼58% of its volume filled would be ideal; however, it may require reoptimization of reaction conditions due to their poor translation with change in batch reactor volume.[41] Section 3 in SI provides additional details on production scenarios. The flexibility and modular configuration of flow reactors opens pathways for cost-efficient and industrial scale manufacturing of novel MOFs.

CONCLUSIONS

An optimized flow synthesis procedure permits the accelerated manufacturing of Ni_2Cl_2(BTDD): a strong candidate for adsorption-based atmospheric water capture platforms. Process parameters such as residence time, reaction temperature, and solvent quantity were optimized by mapping the chemical synthesis space of Ni_2Cl_2(BTDD). Ideal synthesis conditions in flow resulted in reduced methanol and hydrochloric acid volumes in the precursor mixture by 50% and 40%, respectively, while achieving a 3-fold increase in productivity in comparison to batch synthesis. Trade-offs associated with using larger tube sizes on process productivity and deteriorating heat transfer properties were evaluated using a CFD model. These results represent a critical advance toward realizing a sustainable and scalable manufacturing route for Ni_2Cl_2(BTDD); they also provide a potential blueprint for the production of other azolate-based, water-stable MOFs that may impact atmospheric water generation technologies and other applications requiring water stability and high porosity.

ASSOCIATED CONTENT

Supporting Information

The Supporting Information is available free of charge at https://pubs.acs.org/doi/10.1021/acssuschemeng.0c07055.

Detailed description of flow synthesis platform, all materials and experimental methods, reactor operational parameters, and scale-up estimates are provided (PDF)

Crystalline MOF particles exiting the reactor (MP4)

AUTHOR INFORMATION

Corresponding Author

Yuriy Román-Leshkov − *Department of Chemical Engineering, Massachusetts Institute of Technology, Cambridge, Massachusetts 02139, United States;* orcid.org/0000-0002-0025-4233; Phone: 617.253.7090; Email: yroman@mit.edu; Fax: 617.253.7090

Authors

Sujay Bagi − *Department of Mechanical Engineering and Department of Chemical Engineering, Massachusetts Institute of Technology, Cambridge, Massachusetts 02139, United States*

Ashley M. Wright − *Department of Chemistry, Massachusetts Institute of Technology, Cambridge, Massachusetts 02139, United States;* orcid.org/0000-0002-9475-2638

Julius Oppenheim − *Department of Chemistry, Massachusetts Institute of Technology, Cambridge, Massachusetts 02139, United States*

Mircea Dincă − *Department of Chemistry, Massachusetts Institute of Technology, Cambridge, Massachusetts 02139, United States*

Complete contact information is available at: https://pubs.acs.org/10.1021/acssuschemeng.0c07055

Notes

The authors declare no competing financial interest.

ACKNOWLEDGMENTS

S.B. and Y.R-L., thank the U.S. Department of Energy, Office of Basic Energy Sciences under Award No. DE-SC0016214 for support. The authors would like to thank Dr. Charles Settens for fruitful discussion related to quantification of relative crystallinity using PXRD data and Dr. Yong Zhang for technical assistance with TEM.

REFERENCES

(1) Wang, S. B.; Peng, Y. L. Natural zeolites as effective adsorbents in water and wastewater treatment. *Chem. Eng. J.* **2010**, *156* (1), 11−24.

(2) Rieth, A. J.; Dincă, M. Moisture Farming with Metal-Organic Frameworks. *Chem.* **2017**, *2* (6), 757−759.

(3) Jenkins, B.; Gilbert, R.; Nelson, J. *2030 Water Resources Group: Collaboration and Country Leadership to Strengthen Water Security* 2017. https://www.hks.harvard.edu/sites/default/files/2030%20WRG%20final.pdf.

(4) Jenkins, B. R. Decision Making for Sustainability. *Glob Iss Water Pol* **2018**, *19*, 377−430.

(5) Kim, H.; Yang, S.; Rao, S. R.; Narayanan, S.; Kapustin, E. A.; Furukawa, H.; Umans, A. S.; Yaghi, O. M.; Wang, E. N. Water harvesting from air with metal-organic frameworks powered by natural sunlight. *Science* **2017**, *356* (6336), 430−432.
(6) Schneider, S. H. *Encyclopedia of climate and weather*. Oxford University Press: 2011; Vol. *1*. doi: DOI: 10.1093/acref/9780199765324.001.0001.
(7) Wei, R. P.; Gaggioli, C. A.; Li, G. Z.; Islamoglu, T.; Zhang, Z. X.; Yu, P.; Farha, O. K.; Cramer, C. J.; Gagliardi, L.; Yang, D.; Gates, B. C. Tuning the Properties of Zr6O8 Nodes in the Metal Organic Framework UiO-66 by Selection of Node-Bound Ligands and Linkers. *Chem. Mater.* **2019**, *31* (5), 1655−1663.
(8) Wright, A. M.; Rieth, A. J.; Yang, S.; Wang, E. N.; Dincă, M. Precise control of pore hydrophilicity enabled by post-synthetic cation exchange in metal−organic frameworks. *Chem. Sci.* **2018**, *9* (15), 3856−3859.
(9) Rieth, A. J.; Hunter, K. M.; Dinca, M.; Paesani, F., Hydrogen bonding structure of confined water templated by a metal-organic framework with open metal sites. *Nat. Commun.* **2019**, *10*. doi: DOI: 10.1038/s41467-019-12751-z.
(10) Rieth, A. J.; Wright, A. M.; Skorupskii, G.; Mancuso, J. L.; Hendon, C. H.; Dinca, M. Record-Setting Sorbents for Reversible Water Uptake by Systematic Anion Exchanges in Metal-Organic Frameworks. *J. Am. Chem. Soc.* **2019**, *141* (35), 13858−13866.
(11) Rieth, A. J.; Yang, S.; Wang, E. N.; Dinca, M. Record Atmospheric Fresh Water Capture and Heat Transfer with a Material Operating at the Water Uptake Reversibility Limit. *ACS Cent. Sci.* **2017**, *3* (6), 668−672.
(12) Canivet, J.; Bonnefoy, J.; Daniel, C.; Legrand, A.; Coasne, B.; Farrusseng, D. Structure-property relationships of water adsorption in metal-organic frameworks. *New J. Chem.* **2014**, *38* (7), 3102−3111.
(13) Coasne, B.; Gubbins, K. E.; Pellenq, R. J. M. Temperature effect on adsorption/desorption isotherms for a simple fluid confined within various nanopores. *Adsorption* **2005**, *11*, 289−294.
(14) Zhou, H. C.; Long, J. R.; Yaghi, O. M. Introduction to Metal-Organic Frameworks. *Chem. Rev.* **2012**, *112* (2), 673−674.
(15) Monsalve-Bravo, G. M.; Moscoso-Vasquez, H. M.; Alvarez, H. Scaleup of Batch Reactors Using Phenomenological-Based Models. *Ind. Eng. Chem. Res.* **2014**, *53* (22), 9439−9453.
(16) Liu, Z. D.; Zhu, J.; Wakihara, T.; Okubo, T. Ultrafast synthesis of zeolites: breakthrough, progress and perspective. *Inorg. Chem. Front.* **2019**, *6* (1), 14−31.
(17) Liu, Z. D.; Zhu, J.; Peng, C.; Wakihara, T.; Okubo, T. Continuous flow synthesis of ordered porous materials: from zeolites to metal-organic frameworks and mesoporous silica. *React. Chem. Eng.* **2019**, *4* (10), 1699−1720.
(18) Steinbacher, J. L.; McQuade, D. T. Polymer chemistry in flow: New polymers, beads, capsules, and fibers. *J. Polym. Sci., Part A: Polym. Chem.* **2006**, *44* (22), 6505−6533.
(19) Kim, H.; Nagaki, A.; Yoshida, J., A flow-microreactor approach to protecting-group-free synthesis using organolithium compounds. *Nat. Commun.* **2011**, *2*. doi: DOI: 10.1038/ncomms1264.
(20) Adamo, A.; Beingessner, R. L.; Behnam, M.; Chen, J.; Jamison, T. F.; Jensen, K. F.; Monbaliu, J. C. M.; Myerson, A. S.; Revalor, E. M.; Snead, D. R.; Stelzer, T.; Weeranoppanant, N.; Wong, S. Y.; Zhang, P. On-demand continuous-flow production of pharmaceuticals in a compact, reconfigurable system. *Science* **2016**, *352* (6281), 61−67.
(21) Yoshida, J. I.; Kim, H.; Nagaki, A. Green and Sustainable Chemical Synthesis Using Flow Microreactors. *ChemSusChem* **2011**, *4* (3), 331−340.
(22) Pieber, B.; Shalom, M.; Antonietti, M.; Seeberger, P. H.; Gilmore, K. Continuous Heterogeneous Photocatalysis in Serial Micro-Batch Reactors. *Angew. Chem., Int. Ed.* **2018**, *57* (31), 9976−9979.
(23) Batten, M. P.; Rubio-Martinez, M.; Hadley, T.; Carey, K. C.; Lim, K. S.; Polyzos, A.; Hill, M. R. Continuous flow production of metal-organic frameworks. *Curr. Opin. Chem. Eng.* **2015**, *8*, 55−59.
(24) Reinsch, H.; Waitschat, S.; Chavan, S. M.; Lillerud, K. P.; Stock, N. A Facile "Green" Route for Scalable Batch Production and Continuous Synthesis of Zirconium MOFs. *Eur. J. Inorg. Chem.* **2016**, *27*, 4490−4498.
(25) Rubio-Martinez, M.; Avci-Camur, C.; Thornton, A. W.; Imaz, I.; Maspoch, D.; Hill, M. R. New synthetic routes towards MOF production at scale. *Chem. Soc. Rev.* **2017**, *46* (11), 3453−3480.
(26) Waitschat, S.; Wharmby, M. T.; Stock, N. Flow-synthesis of carboxylate and phosphonate based metal-organic frameworks under non-solvothermal reaction conditions. *Dalton T* **2015**, *44* (24), 11235−11240.
(27) Albuquerque, G. H.; Fitzmorris, R. C.; Ahmadi, M.; Wannenmacher, N.; Thallapally, P. K.; McGrail, B. P.; Herman, G. S. Gas−liquid segmented flow microwave-assisted synthesis of MOF-74(Ni) under moderate pressures. *CrystEngComm* **2015**, *17* (29), 5502−5510.
(28) Rasmussen, E. G.; Kramlich, J.; Novosselov, I. V. Scalable Continuous Flow Metal−Organic Framework (MOF) Synthesis Using Supercritical CO2. *ACS Sustainable Chem. Eng.* **2020**, *8* (26), 9680−9689.
(29) Gao, H.; Luan, Y.; Chaikittikul, K.; Dong, W.; Li, J.; Zhang, X.; Jia, D.; Yang, M.; Wang, G. A Facile in Situ Self-Assembly Strategy for Large-Scale Fabrication of CHS@MOF Yolk/Shell Structure and Its Catalytic Application in a Flow System. *ACS Appl. Mater. Interfaces* **2015**, *7* (8), 4667−4674.
(30) He, B.; Sadiq, M. M.; Batten, M. P.; Suzuki, K.; Rubio-Martinez, M.; Gardiner, J.; Hill, M. R. Continuous Flow Synthesis of a Zr Magnetic Framework Composite for Post-Combustion CO2 Capture. *Chem. - Eur. J.* **2019**, *25* (57), 13184−13188.
(31) Bayliss, P. A.; Ibarra, I. A.; Perez, E.; Yang, S. H.; Tang, C. C.; Poliakoff, M.; Schroder, M. Synthesis of metal-organic frameworks by continuous flow. *Green Chem.* **2014**, *16* (8), 3796−3802.
(32) Kashid, M. N.; Agar, D. W. Hydrodynamics of liquid-liquid slug flow capillary microreactor: Flow regimes, slug size and pressure drop. *Chem. Eng. J.* **2007**, *131* (1−3), 1−13.
(33) Ghaini, A.; Mescher, A.; Agar, D. W. Hydrodynamic studies of liquid-liquid slug flows in circular microchannels. *Chem. Eng. Sci.* **2011**, *66* (6), 1168−1178.
(34) Song, H.; Chen, D. L.; Ismagilov, R. F. Reactions in droplets in microflulidic channels. *Angew. Chem., Int. Ed.* **2006**, *45* (44), 7336−7356.
(35) Jovanovic, J.; Zhou, W. Y.; Rebrov, E. V.; Nijhuis, T. A.; Hessel, V.; Schouten, J. C. Liquid-liquid slug flow: Hydrodynamics and pressure drop. *Chem. Eng. Sci.* **2011**, *66* (1), 42−54.
(36) Ufer, A.; Mendorf, M.; Ghaini, A.; Agar, D. W. Liquid-Liquid Slug Flow Capillary Microreactor. *Chem. Eng. Technol.* **2011**, *34* (3), 353−360.
(37) Patterson, J. P.; Abellan, P.; Denny, M. S.; Park, C.; Browning, N. D.; Cohen, S. M.; Evans, J. E.; Gianneschi, N. C. Observing the Growth of Metal-Organic Frameworks by in Situ Liquid Cell Transmission Electron Microscopy. *J. Am. Chem. Soc.* **2015**, *137* (23), 7322−7328.
(38) Gunther, A.; Jensen, K. F. Multiphase microfluidics: from flow characteristics to chemical and materials synthesis. *Lab Chip* **2006**, *6* (12), 1487−1503.
(39) Sonneveld, E. J.; Visser, J. W. Automatic Collection of Powder Data from Photographs. *J. Appl. Crystallogr.* **1975**, *8* (Feb1), 1−7.
(40) Dunne, P. W.; Lester, E.; Walton, R. I. Towards scalable and controlled synthesis of metal-organic framework materials using continuous flow reactors. *React. Chem. Eng.* **2016**, *1* (4), 352−360.
(41) Rubio-Martinez, M.; Hadley, T. D.; Batten, M. P.; Constanti-Carey, K.; Barton, T.; Marley, D.; Monch, A.; Lim, K. S.; Hill, M. R. Scalability of Continuous Flow Production of Metal-Organic Frameworks. *ChemSusChem* **2016**, *9* (9), 938−941.
(42) Plutschack, M. B.; Pieber, B.; Gilmore, K.; Seeberger, P. H. The Hitchhiker's Guide to Flow Chemistry(II). *Chem. Rev.* **2017**, *117* (18), 11796−11893.
(43) Tummala, S.; Ramirez, A.; Srivastava, S.; Hallow, D. M. DEVELOPMENT OF DESIGN SPACE FOR REACTION STEPS:

https://dx.doi.org/10.1021/acssuschemeng.0c07055
ACS Sustainable Chem. Eng. XXXX, XXX, XXX−XXX

APPROACHES AND CASE STUDIES FOR IMPURITY CONTROL. *Chemical Engineering in the Pharmaceutical Industry: Active Pharmaceutical Ingredients* **2019**, 1091−1122.
(44) Illg, T.; Lob, P.; Hessel, V. Flow chemistry using milli- and microstructured reactors-From conventional to novel process windows. *Bioorg. Med. Chem.* **2010**, *18* (11), 3707−3719.
(45) Gómez-Gualdrón, D. A.; Moghadam, P. Z.; Hupp, J. T.; Farha, O. K.; Snurr, R. Q. Application of Consistency Criteria To Calculate BET Areas of Micro- And Mesoporous Metal−Organic Frameworks. *J. Am. Chem. Soc.* **2016**, *138* (1), 215−224.
(46) Rieth, A. J.; Dinca, M. Controlled Gas Uptake in Metal-Organic Frameworks with Record Ammonia Sorption. *J. Am. Chem. Soc.* **2018**, *140* (9), 3461−3466.
(47) Dinca, M.; Rieth, A. J.; Tulchinsky, Y. *Compositions comprising metal organic frameworks for the uptake of compounds and related methods* 2017. https://patents.google.com/patent/US10653993B2/en.
(48) Furukawa, H.; Cordova, K. E.; O'Keeffe, M.; Yaghi, O. M. The Chemistry and Applications of Metal-Organic Frameworks. *Science* **2013**, *341* (6149), 974.
(49) Czaja, A. U.; Trukhan, N.; Muller, U. Industrial applications of metal-organic frameworks. *Chem. Soc. Rev.* **2009**, *38* (5), 1284−1293.
(50) Barthe, P.; Guermeur, C.; Lobet, O.; Moreno, M.; Woehl, P.; Roberge, D. M.; Bieler, N.; Zimmermann, B. Continuous multi-injection reactor for multipurpose production - Part I. *Chem. Eng. Technol.* **2008**, *31* (8), 1146−1154.
(51) Zhang, J.; Wang, K.; Teixeira, A. R.; Jensen, K. F.; Luo, G. Design and Scaling Up of Microchemical Systems: A Review. *Annu. Rev. Chem. Biomol. Eng.* **2017**, *8* (1), 285−305.
(52) Eesa, M.; Barigou, M. CFD Simulation of Transverse Vibration Effects on Radial Temperature Profile and Thermal Entrance Length in Laminar Flow. *AIChE J.* **2011**, *57* (1), 51−56.
(53) Toh, K. H.; Ghajar, A. J. Heat-Transfer in the Thermal Entrance Region for Viscoelastic Fluids in Turbulent Pipe Flows. *Int. J. Heat Mass Transfer* **1988**, *31* (6), 1261−1267.

https://dx.doi.org/10.1021/acssuschemeng.0c07055
ACS Sustainable Chem. Eng. XXXX, XXX, XXX−XXX